Geoscience Frontiers xxx (2018) 1–12

HOSTED BY

ELSEVIER

Contents lists available at ScienceDirect

China University of Geosciences (Beijing)

Geoscience Frontiers

journal homepage: www.elsevier.com/locate/gsf

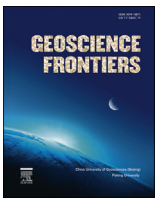

Research Paper

The role of carbonate-fluoride melt immiscibility in shallow REE deposit evolution

Jindrich Kynicky [a,b,*], Martin P. Smith [c], Wenlei Song [a], Anton R. Chakhmouradian [d], Cheng Xu [e], Antonin Kopriva [a], Michaela Vasinova Galiova [a], Martin Brtnicky [a]

[a] Mendel University in Brno, Zemedelska 1, 613 00 Brno, Czech Republic
[b] Central European Institute of Technology, Brno University of Technology, Technicka 3058/10, 616 00 Brno, Czech Republic
[c] University of Brighton, Brighton BN2 4GJ, United Kingdom
[d] University of Manitoba, Winnipeg, Manitoba, Canada
[e] School of Earth and Space Sciences, Peking University, Beijing 100871, China

ARTICLE INFO

Article history:
Received 5 August 2017
Received in revised form
11 December 2017
Accepted 7 February 2018
Available online xxx
Handling Editor: Nick M. W. Roberts

Keywords:
Silicate-carbonate-fluoride melt immiscibility
Carbonatite
Alkaline syenite
Shallow REE deposit
Lugiin Gol
Mongolia

ABSTRACT

The Lugiin Gol nepheline syenite intrusion, Mongolia, hosts a range of carbonatite dikes mineralized in rare-earth elements (REE). Both carbonatites and nepheline syenite-fluorite-calcite veinlets are host to a previously unreported macroscale texture involving pseudo-graphic intergrowths of fluorite and calcite. The inclusions within calcite occur as either pure fluorite, with associated REE minerals within the surrounding calcite, or as mixed calcite-fluorite inclusions, with associated zirconosilicate minerals. Consideration of the nature of the texture, and the proportions of fluorite and calcite present (~29 and 71 mol%, respectively), indicates that these textures most likely formed either through the immiscible separation of carbonate and fluoride melts, or from cotectic crystallization of a carbonate-fluoride melt. Laser ablation ICP-MS analyses show the pure fluorite inclusions to be depleted in REE relative to the calcite. A model is proposed, in which a carbonate-fluoride melt phase enriched in Zr and the REE, separated from a phonolitic melt, and then either unmixed or underwent cotectic crystallization to generate an REE-rich carbonate melt and an REE-poor fluoride phase. The separation of the fluoride phase (either solid or melt) may have contributed to the enrichment of the carbonate melt in REE, and ultimately its saturation with REE minerals. Previous data have suggested that carbonate melts separated from silicate melts are relatively depleted in the REE, and thus melt immiscibility cannot result in the formation of REE-enriched carbonatites. The observations presented here provide a mechanism by which this could occur, as under either model the textures imply initial separation of a mixed carbonate-fluoride melt from a silicate magma. The separation of an REE-enriched carbonate-fluoride melt from phonolitic magma is a hitherto unrecognized mechanism for REE-enrichment in carbonatites, and may play an important role in the formation of shallow magmatic REE deposits.

1. Introduction

Carbonate igneous rocks accounted for the bulk of global production of rare-earth elements (REE) between the early 1960s, when the Mountain Pass mine in California went on stream, and the late 1980s, when the Bayan Obo mine in China became a major REE producer (Kynicky et al., 2012; Mariano and Mariano, 2012; Chakhmouradian et al., 2015). Today, 40% or more of advanced REE exploration projects worldwide still target carbonatites and related rocks (Chakhmouradian and Wall, 2012; Cox and Kynicky, 2017). For this reason, a more detailed understanding of the petrogenesis of these deposits is desirable, from both scientific and exploration viewpoints. In 1971, a Russian geological expedition discovered the Lugiin Gol nepheline syenite complex in Mongolia (Fig. 1). Little geochemical work has been carried out on this intrusion, with only basic petrological and geochemical data on the carbonatites reported (Kovalenko et al., 1974; Kynicky, 2006; Baatar et al., 2013). However, new fieldwork and petrographic analysis

* Corresponding author. Mendel University in Brno, Zemedelska 1, 613 00 Brno, Czech Republic.
E-mail address: jindrak@email.cz (J. Kynicky).
Peer-review under responsibility of China University of Geosciences (Beijing).

https://doi.org/10.1016/j.gsf.2018.02.005

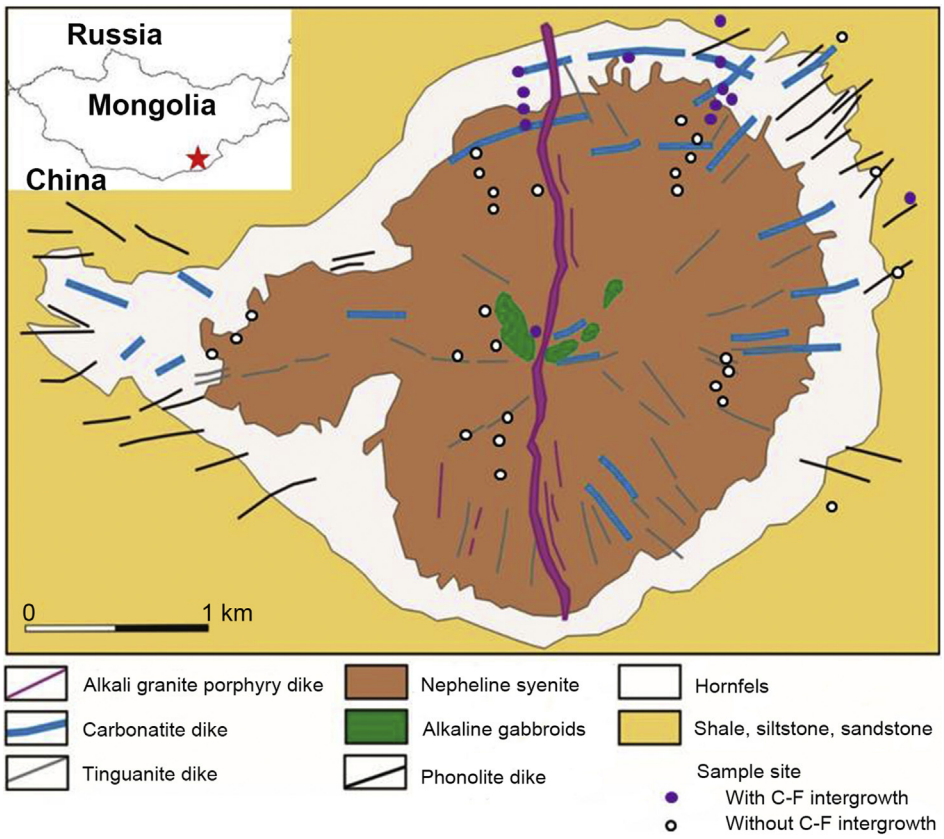

Figure 1. Sketch map of the Lugiin Gol alkaline igneous complex, based on Batbold (1997).

have uncovered a number of remarkable features that have bearing on the evolution of alkaline igneous systems enriched in rare metals (in particular, REE and high-field-strength elements). This paper reports unique calcite-fluorite intergrowth textures from the Lugiin Gol carbonatites, and examines the co-existence of REE-rich carbonatites and fluorite-rich rocks. Results of the study provide new insights into the role of melt immisciblity in the formation of REE deposits spatially related to shallow intrusions of peralkaline melts, where multistage silicate-carbonate-fluoride melt immiscibility may be a previously unrecognized, but extremely important process in the generation of REE-mineralized carbonatites.

2. Melt immiscibility in alkaline magmatism

Liquid-liquid immiscibility is a relatively widespread process in magmatic systems. In alkaline igneous systems, the immiscible separation of a carbonate fraction from alkaline melts of phonolitic to nephelinitic composition has been identified as a viable mechanism in the genesis of some carbonatites (e.g., Lee and Wyllie, 1997, 1998; Bell, 1998; Harmer, 1999; Halama et al., 2005; Panina, 2005; Mitchell and Dawson, 2012; Veksler et al., 2012), with the onset of immiscibility estimated to occur over a range of T and P depending on the degree of CO_2 saturation in the melt (Brooker and Kjarsgaard, 2011). However, despite experimental and field-based studies, which indicate that immiscibility should occur between silicate and a range of salt melts (Veksler, 2004), and between Ca-carbonate and Na-carbonate or chloride melts (Fulignati et al., 2001; Mitchell and Kjarsgaard, 2008), and the widespread occurrence of fluorine as a lithophile halogen in igneous systems, silicate-fluoride melt immiscibility has been found in only a limited number of studies (Veksler et al., 2005; Vasyukova and Williams-Jones, 2014). Low-T (<980 °C) carbonate-halide immiscibility has been documented by Panina (2005) in melt inclusions hosted by silicate minerals from alkali-ultramafic rocks associated with carbonatites, and by Mitchell (1997) in natrocarbonatite lava. Immiscibility potentially has great importance for the development of rare-metal deposits in igneous systems because the REE have been shown to partition into fluoride melts relative to their conjugate silicate melts (Veksler et al., 2012; Vasyukova and Williams-Jones, 2014), but in silicate-carbonate systems, these elements (alongside Nb, Zr, Th and U) appear to favour the silicate phase. This means that carbonatites associated with economic REE deposits may have evolved via mechanisms other than immiscibility in order to attain high levels of REE enrichment (Le Bas, 1987; Harmer, 1999; Bell and Rukhlov, 2004; Mitchell, 2005).

3. Geological outline of Lugiin Gol complex

The Lugiin Gol Complex is situated in the Lugiin Gol district (geographic coordinates: 42°58′45″–42°56′50″N, 108°32′02″–108°36′50″E) in the south-eastern part of the Caledonian Gobi-Tien Shan Fold Belt, South Mongolia (Fig. 1). It consists of a nepheline syenite composite pluton and associated dike rocks emplaced near the boundary between the Belt and the Sulinkheer suture zone into Late Permian black shales of the Lugiin Gol Formation (Kovalenko et al., 1974).

The massif consists of a nepheline syenite stock and equivalent dike rocks in an area of approximately 13 km^2, showing an elongated circular outline with diameter of almost 4 km (Fig. 1). Contacts are relatively sharp, and the country rock is thermally metamorphosed to fine grained hornfels with a width near 500 m for the most parts, but in the western part of complex the width of the hornfels reaches 1650 m. Tinguaite (hypabyssal phonolite) and carbonatite dykes occur in a partly concentric, but dominantly

Please cite this article in press as: Kynicky, J., et al., The role of carbonate-fluoride melt immiscibility in shallow REE deposit evolution, Geoscience Frontiers (2018), https://doi.org/10.1016/j.gsf.2018.02.005

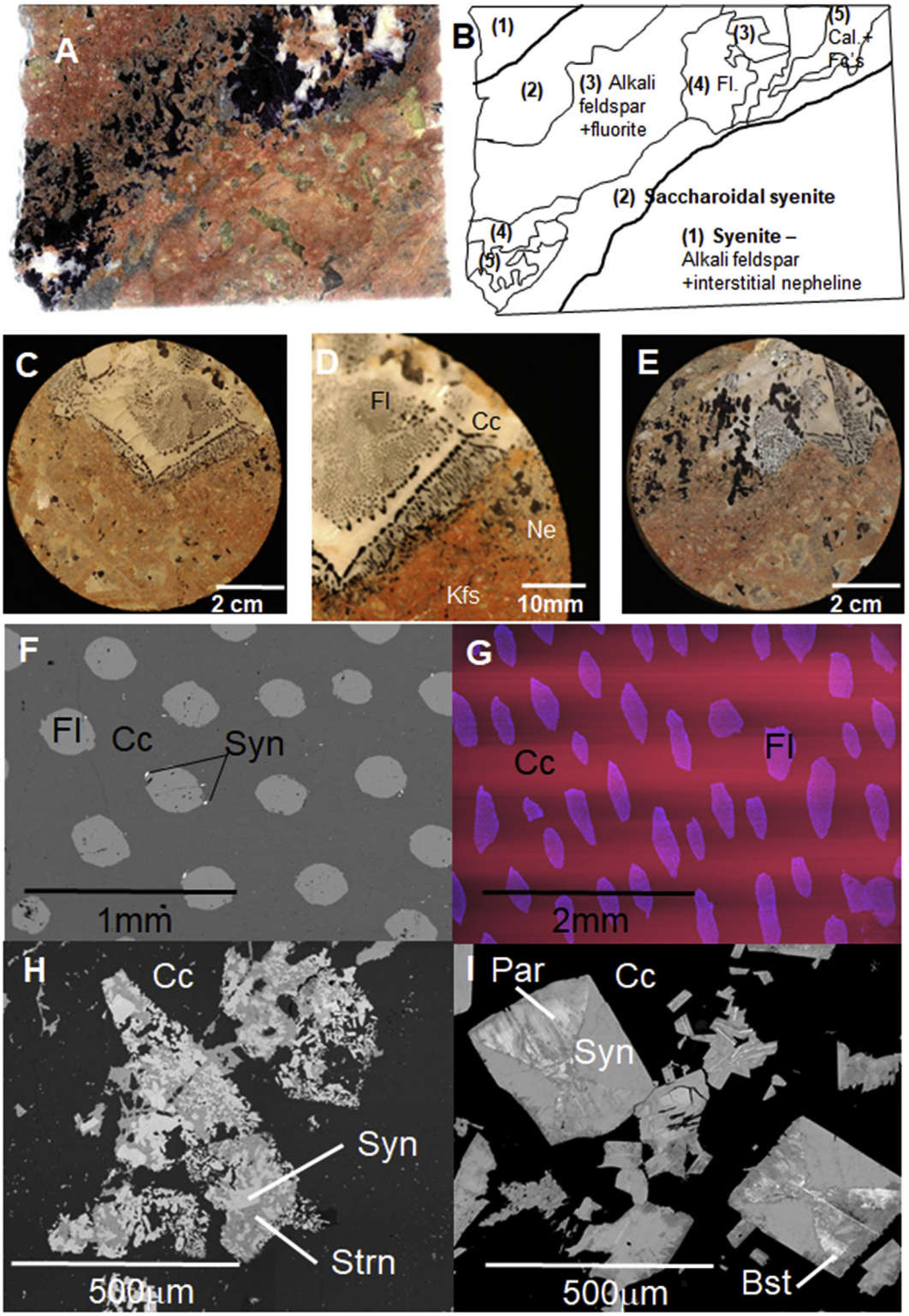

Figure 2. Representative images of composite carbonatite-syenite dikes and calcite-fluorite intergrowth textures. (A) and (B) Photograph and interpretive sketch of a longitudinal core section showing a feldspar-fluorite calcite dyke cutting nepheline syentite. This dyke includes both feldspar-fluorite and calcite-fluorite intergrowths and is representative of the structures hosting graphic calcite-fluorite intergrowth; (C–E) Representative images of calcite-fluorite intergrowth texture at a range of scales; (F) Backscattered electron image of fluorite blebs in calcite; (G) Cathode-luminescence image of fluorite blebs in calcite; (H) Backscattered electron image of synchysite-(Ce) and strontianite replacing burbankite-(Ce) in carbonatite; (I) BSE image of synchysite-(Ce), parisite-(Ce) and bastnasite-(Ce) in carbonatite. Fl–fluorite; Cc–calcite; Syn–synchysite-(Ce); Par–parisite-(Ce); Bst–bastnäsite-(Ce); Strn–Strontianite.

radial structure. The carbonatite dykes consist of calcite, strontianite, apatite, burbankite, fluorite, REE-flurocarbonates, monazite, barite, celestine, pyrite, sphalerite, galenite, molybdenite, and tens of other rarer accessories. Twenty-one representative carbonatite samples from both outrops and currently obtained drill cores were selected for detailed whole rock and minerals analyses.

The Lugiin Gol carbonatites are not as common or volumetrically significant as the alkaline silicate rocks (syenites) but

Please cite this article in press as: Kynicky, J., et al., The role of carbonate-fluoride melt immiscibility in shallow REE deposit evolution, Geoscience Frontiers (2018), https://doi.org/10.1016/j.gsf.2018.02.005

represent the only source of unique REE mineralization amenable to extraction and metal recovery among the presently known occurrences and deposits of REE ores in Mongolia. Although the carbonatites show much variation in mineralogical and petrographical characteristics, they can be generally categorized as intrusive calcite carbonatites (sövites). These rocks occur predominantly as dikes and veins ranging from a few centimeters to 2 m in width, and reaching 1000 m in length. All carbonatites are medium- to coarse-grained massive rocks and consist predominantly of calcite. Calcite is medium- to coarse-grained (0.1–15 mm) and forms a mosaic of anhedral crystals (70%–98%) associated with accessory amounts of primary euhedral apatite or REE carbonates.

Based on mineralogical and textural criteria, the following three types of primary carbonatite can be distinguished:

(1) Inequigranular, locally laminated allotriomorphic carbonatites with euhedral hexagonal crystals of burbankite [$(Na,Ca)_3(Sr,Ba,Ce)_3(CO_3)_5$] up to 2 cm × 3 cm in size, either fresh or pseudomorphed by an assemblage of late-stage carbonates (±sulphates). Fluorite is a common accessory phase, although typically not as abundant as burbankite (≤5 vol.% and 30 vol.%, respectively). Fluorite occurs as a skeletal crystals of purple colour and "graphic" intergrowths with calcite up to 5 cm in size (Fig. 2). This type of carbonatite is characteristically enriched in sulfides (predominantly pyrite, ≤5 vol.%, associated with sphalerite, ≤1 vol.% and rare chalcopyrite and molybdenite).
(2) Near monomineralic massive, coarse-grained to pegmatoid carbonatites comprising predominantly of calcite (≥95 vol.%) with minor fluorapatite and negligible amounts of other accessory minerals.
(3) Coarse-grained to pegmatoid carbonatites containing abundant prismatic crystals up to 15 mm in length, radiating and stellate aggregates of REE fluorcarbonates ranging from 10 to 25 vol.%. Commonly, smaller synchysite-Ce crystals (synchysite II) of similar habit but with less evolved pinacoidal sectors of exclusively parisite-(Ce) decorate the margins of calcite crystals in association with strontianite and Fe-, Mg-, Mn-bearing ternary carbonates (±pyrite).

Several dikes are zoned and exhibit a pegmatoid texture. The selvage of these zoned bodies comprises fine-grained calcite and fluorite and is practically devoid of fluorcarbonates. This zone grades through the medium- to coarse-grained (locally extremely so) burbankite bearing zone also containing primary fluorcarbonate crystals. The primary mineral associations and textural relations are altered by hydrothermal reworking, particularly in the apical parts of the pluton. The most typical products of this reworking are complex pseudomorphs after the primary burbankite, fluorite stringers interrupting the igneous texture, and newly-formed ancylite-(Ce) developed along fractures, commonly in association with barite and/or celestine.

4. Material and analytical methods

Representative carbonatite samples from both outcrops and recent drill core material were selected for detailed analysis using a variety of instrumental techniques. Of totally 21 samples, 15 were used for detailed analysis of the composition of major and accessory minerals, and 8 were used for detailed analysis of calcite fluroite intergrowths.

Mineral identification and petrographic characterization were based on microscopic observations in plane- and cross-polarized transmitted light, back scattered electron (BSE) and cathodoluminescence (CL) imaging combined with energy-dispersive X-ray spectrometry (EDS). All 15 samples were analysed with a conductive carbon layer (thickness of 10 nm) in the High Vacuum Mode at typical working conditions – accelerating voltage 25 kV, working distance 15 mm.

The chemical composition of major and accessory minerals from 15 representative samples of Lugiin Gol carbonatites were determined by wavelength-dispersive X-ray spectrometry (WDS) using a Cameca SX 100 electron microprobe at the Joint Electron Microscopy and Microanalysis Laboratory (Institute of Geological Sciences, Masaryk University and Czech Geological Survey, Czech Republic). The instrument was operated at a beam current of 10 nA and an accelerating voltage of 15 kV. The electron beam was defocused to a spot size of 5–10 μm to minimize beam-induced damage and thermal decomposition of such heat-sensitive mineral phases as carbonates. The following standards and X-ray emission lines were used in the analysis of calcite: dolomite (Mg, Kα), calcite (Ca, Kα), willemite (Mn, Kα), olivine (Fe, Kα) and celestine (Sr, Lα). For the analysis of feldspar, albite (Na, Kα), sanidine (Al, Si and K, Kα line for all), celestine (Sr, Lα), barite (Ba, Lα) and andradite (Fe, Kα) were used. For the analysis of REE bearing minerals, andradite (Si and Fe, Kα line for both), wollastonite (Ca, Kα), apatite (P, Kα), barite (S, Kα), celestine (Sr, Lα), topaz (F, Kα), synthetic ThO_2 (Th, Mα) and U (U, Mβ), galena (Pb, Mα), Y-Al garnet (Y, Kα), REE glasses and orthophosphates (La, Ce and Sm with Lα line; Pr, Nd, Gd and Dy with Lβ) were used. The data were reduced and corrected using the PAP routine of Pouchou and Pichoir (1991).

Trace-element analysis of selected Ca- and Ca-Sr-REE carbonate minerals and fluorite by laser-ablation inductively-coupled-plasma mass-spectrometry (ICP-MS) was performed at the Laboratory of Atomic Spectrochemistry, Masaryk University, using an Agilent 7500ce spectrometer and a UP-213 pulsed Nd:YAG laser system operated at a wavelength of 213 nm and pulse duration of 4.2 ns. This ablation system is equipped with a SuperCell sample chamber (New Wave Research) designed for rapid evacuation of the laser-generated aerosol. Helium was used as a carrier gas with a flow rate of 1 L/min. The samples were analysed using a spot diameter of 55 μm, dwell time of 60 s, repetition rate of 10 Hz and fluence of 5 J/cm^2. The calcium content determined by WDS was used as an internal standard, and external calibration was performed using glass standard NIST 610. The analytical method for laser-ablation ICP-MS is described in detail in Xu et al. (2015).

5. Results

5.1. "Graphic" calcite-fluorite intergrowths

All samples examined in detail showed "graphic" calcite-fluorite intergrowths hosted by either syenite or carbonatite (Fig. 2A–E). The intergrowths occur across a range of scales, from "drops" a few mm across to segregations 10 cm in diameter. The shape of fluorite macro-inclusions in calcite ranges from near-spherical to elongate and amoeboid. The blebs are either randomly distributed within calcite core zones, or are confined to zones parallel to calcite growth faces (Fig. 2C–E). The fluorite in zones parallel to growth zone faces grades outwards into coarser (up to 1 cm long) fluorite crystals, still showing amoeboid morphology, that are intergrown with calcite or alkali feldspar. In some instances, the host syenite is crosscut by veins 2–3 cm in width, composed of allotriomorphic fluorite–alkali feldspar intergrowth, followed by more massive fluorite, and finally calcite (Fig. 2A and B). There are two inclusion types. Type 1 consists of finely intergrown calcite and fluorite (Fig. 3A, D) associated with intermediate members of the armstrongite-elpidite solid solution and other zirconosilicates (Fig. 3). Isolated areas of pure fluorite, with no associated Zr enrichment, occur as segregations at the margins of the inclusions (Fig. 3G–I). Type 2 inclusions are composed either exclusively of fluorite enclosed within calcite

Please cite this article in press as: Kynicky, J., et al., The role of carbonate-fluoride melt immiscibility in shallow REE deposit evolution, Geoscience Frontiers (2018), https://doi.org/10.1016/j.gsf.2018.02.005

(Fig. 2F), or of fluorite associated with very fine-grained zircon, burbankite and REE ± Ca fluorcarbonates in the host calcite (Fig. 2H and I). Cathodoluminescence imaging revealed no zonation in either calcite or fluorite within the intergrowths (Fig. 2G). The zircon and REE ± Ca fluorcarbonates also occur as coarser-grained, sector-zoned, euhedral to subhedral crystals enclosed in calcite (Fig. 2I), but not within coarser-grained fluorite. Within the zoned crystals of fluorcarbonates, clear prismatic sectors always consist of synchysite-(Ce), whereas turbid brownish pinacoidal sectors consist of either parisite-(Ce) or röntgenite-(Ce) showing lower Ca levels than the synchysite zones (Fig. 2I).

5.2. Mineral chemistry

Representative mineral analyses are tabulated in the Supplemental material file. Cores of calcite grains in carbonatites outside the fluorite-calcite intergrowths show enrichment in light REE (LREE = La–Eu) with no marked anomalies at Eu or Y (when plotted as a pseudo-lanthanide – Bau, 1996). The rims of calcite grains, however, show progressive depletion in the LREE and relative enrichment in the heavy REE (HREE = Gd–Lu), accompanied by the development of a negative Y anomaly relative to Dy and Ho. Coarse fluorite grains outside the intergrowths, conversely, show lower total REE contents with variable LREE to HREE ratios, and marked positive Y anomalies (Figs. 4 and 5). Within the calcite-fluorite intergrowths, the compositional ranges of calcite and fluorite are more limited. Calcite is LREE-enriched with no marked anomalies. Fluorite shows lower total REE contents than calcite, less marked LREE enrichment and a marked positive Y anomaly (Fig. 5B). Synchysite-(Ce) and burbankite are both LREE-dominant, with slightly lower levels of the HREE in the latter mineral (Fig. 5C). These compositional data are summarized in Fig. 5D.

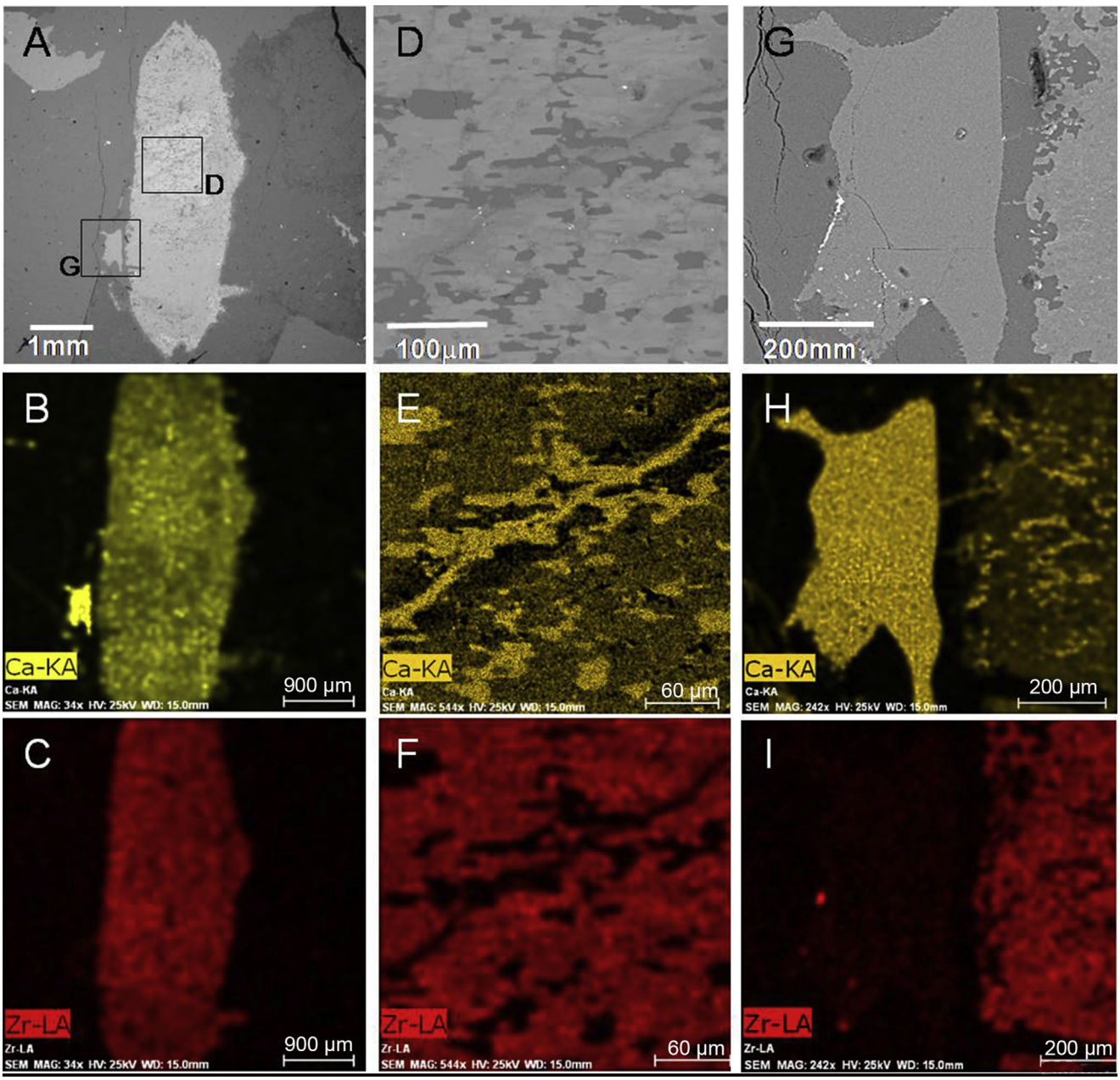

Figure 3. Backscattered electron images and X-ray element maps of type 1 macro-inclusion, showing distribution of fluorite and calcite, and enrichment in Zr. (A–C) Image of whole macro-inclusion; (D–F) Magnified image of (A); (G–I) Margin of (A) showing late development of a fluorite-rich phase, representing the fluoride melt. This lacks significant Zr.

Please cite this article in press as: Kynicky, J., et al., The role of carbonate-fluoride melt immiscibility in shallow REE deposit evolution, Geoscience Frontiers (2018), https://doi.org/10.1016/j.gsf.2018.02.005

6. Discussion

6.1. Significance of calcite-fluorite intergrowths

The closest analogues to the textures described in the present work are vermicular, symplectitic and graphic textures arising from a variety of processes, from eutectic crystallization to liquid immiscibility and subsolidus reactions. Vermicular intergrowths between quartz and sodic feldspar (myrmekite) have been interpreted as subsolidus unmixing of K-bearing plagioclase in the presence of excess Si (Castle and Lindsley, 1993). However, the Lugiin Gol rocks lack an intermediate high-T Ca fluorcarbonate phase, and hence subsolidus unmixing can effectively be ruled out. These textures could also form via reaction between calcite and a HF-bearing fluid. However, symplectitic textures typically arise as a result of diffusion-controlled transport between solid reactants, or between a solid reactant and a grain boundary fluid (Best, 2003). This mechanism is unlikely in our case, where carbonatitic magmas crystallized in a relatively open vein-dike environment, and calcite and fluorite co-precipitated close to equilibrium (Fig. 2C and D). It is also possible that the fluorite represents solid inclusions which precipitated earlier than, and were incorporated into, its associated calcite. Spherical or ovoid fluorite crystals have been reported from quenched run products

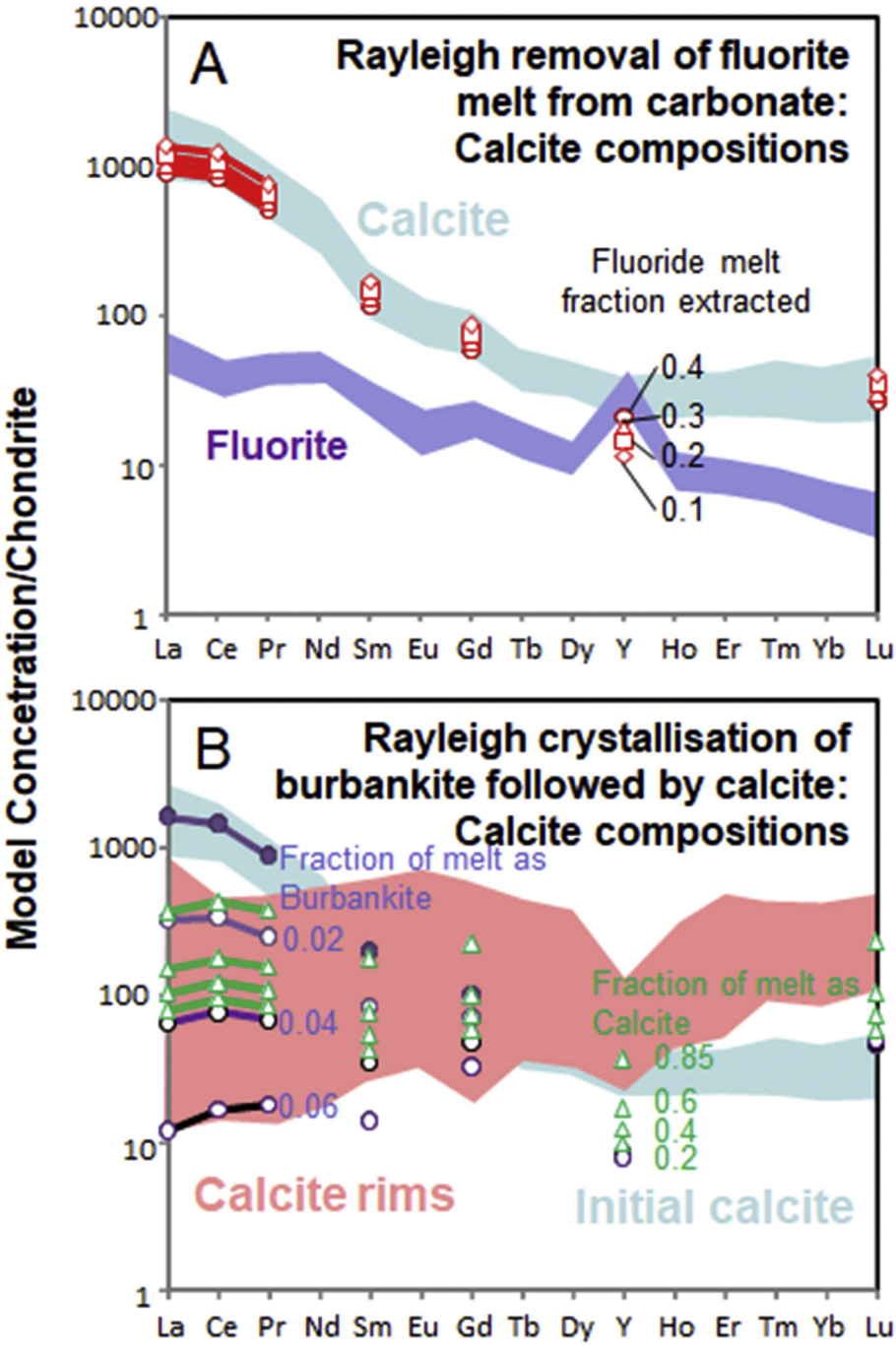

Figure 4. Preliminary model for the evolution of the Lugiin Gol carbonatite via fluorite melt immiscibility (A), followed by crystallisation of an REE-rich mineral phase (B). Both processes are modelled via Rayleigh fractionation. The assumptions and approximations used are detailed in the text. Shaded areas show the range of analytical values obtained by laser ablation ICP-MS (Table 1A and B; Fig. 5).

Please cite this article in press as: Kynicky, J., et al., The role of carbonate-fluoride melt immiscibility in shallow REE deposit evolution, Geoscience Frontiers (2018), https://doi.org/10.1016/j.gsf.2018.02.005

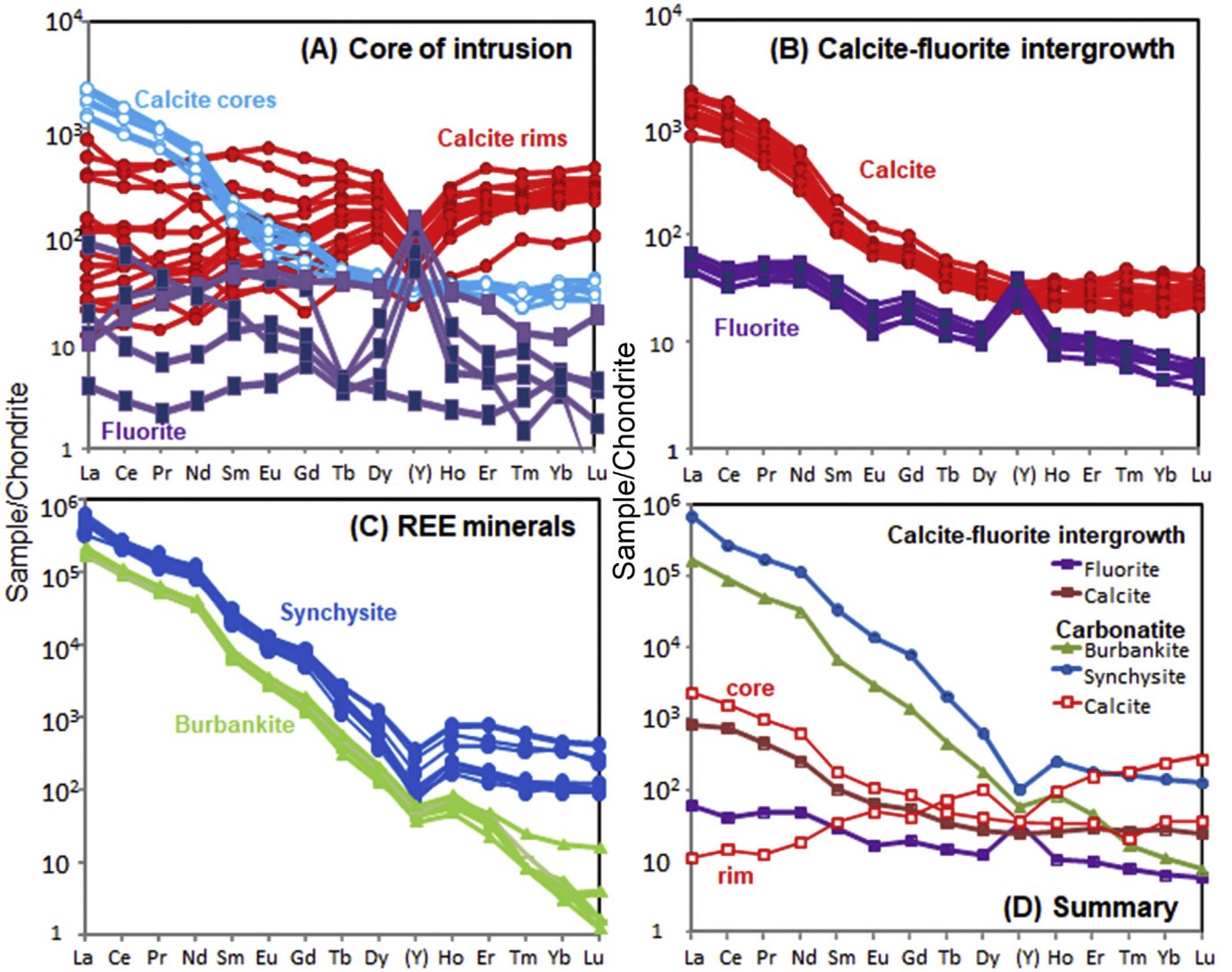

Figure 5. Results of mineral chemical REE analyses from the LuginGol complex. Values normalised to chondrite values of Wakita et al. (1971). (A) Composition of calcite and fluorite from the main intrusion; (B) Composition of calcite and fluorite from intergrowth textures; (C) Composition of synchysite-(Ce) and burbankite-(Ce) from carbonatite; (D) Summary of key features of mineral REE patterns.

in silicate-fluoride melt immiscibility experiments (Veksler, 2004; Veksler et al., 2005). These can be distinguished from true fluoride melt inclusions, as the latter quench to very fine-grained, opaque aggregates rather than transparent single crystals. However, fluoride melt inclusions crystallized to well-formed single crystals have been previously reported in natural rocks (Vasyukova and Williams-Jones, 2014), whereas spherical or ovoid magmatic fluorite has not. The formation of spherical fluorite crystals in experimental melts has not been fully explained, but Veksler (2004) speculated that it may be the result of decrease in excess surface energy between melts and crystals of similar composition. Notably, the Lugiin Gol fluorite inclusions are not hosted by fluoride glass.

The texture described in this work may be more closely analogous to that of graphic granite, although the morphology of the fluorite blebs is significantly different from that of quartz grains in graphic granites. Early work (Fenn, 1986; MacLellan and Trembath, 1991) suggested that the graphic texture formed as a result of simultaneous crystallization close to the eutectic. However, subsequent studies have demonstrated that the modal proportions of graphic-textured material are often significantly removed from the eutectic composition, and proposed models invoking supersaturation at a rapidly growing crystal-melt boundary layer, without the need for eutectic melt compositions (Fenn, 1986). London (2009) further developed this model, and demonstrated that this must entail significant undercooling below the system liquidus ($\sim$200 °C), and required high-viscosity, volatile-poor melts in order to inhibit diffusive and advective transport away from the growth face of the primary phase. In syenites and alkali granites, eutectic temperatures extend from $\sim$1000 °C in dry systems at atmospheric pressure (Schairer, 1957) to below 650 °C in volatile-rich systems at 5 kbar. Given that both silicate and carbonatite melts were emplaced into the same fracture system at Lugiin Gol, significant undercooling is unlikely. Also, the extremely low viscosity of carbonatite melts ($\sim 3–15 \times 10^{-3}$ Pa s at 730–950 °C; Dingwell et al., 2014) in comparison with that of silicic melts developing graphic textures via undercooling (London et al., 2012) makes inhibition of diffusive and advective transport at a crystal growth face unlikely. Thus, the development of calcite-fluorite textures via undercooling does not seem feasible.

Please cite this article in press as: Kynicky, J., et al., The role of carbonate-fluoride melt immiscibility in shallow REE deposit evolution, Geoscience Frontiers (2018), https://doi.org/10.1016/j.gsf.2018.02.005

Table 1A
Spreadsheet showing the model calculations for separation of fluoride melt from carbonate melt, followed by burbankite (Burb) and calcite crystallisation. All processes are assumed to follow Rayleigh fractionation behaviour. All compositional data are chondrite normalised.

	Carbonate melt composition			Calculation of K_d		
	Calcite intergrown with fluorite	K_d Cc/melt[a]	Melt	Fluorite from intergrowths	K_d F-melt/C-melt[b]	K_d C-melt/burb[c]
La	820	0.08	10,302	57	0.005	80.0
Ce	742	0.09	8508	40	0.005	73.3
Pr	455	0.10	4530	47	0.010	64.1
Nd	257			47		63.3
Sm	103	0.14	739	29	0.039	43.8
Eu	64			17		32.2
Gd	54	0.20	274	20	0.075	19.2
Tb	34			14		11.9
Dy	27			12		5.4
Y	24	0.21	118	32	2.500	2.0
Ho	26			10		3.0
Er	29			9		1.4
Tm	27			8		0.8
Yb	28			6		0.3
Lu	24	0.18	138	5	0.039	0.1

[a] Calculated from the data of Dawson and Hinton (2003) and Klemme and Dalpé (2003).
[b] Calculated from the mean fluorite composition and the least evolved carbonate melt composition, assuming fluorite represents the composition of fluoride melt.
[c] Calculated from the mean burbankite composition and the initial carbonate melt composition.

Graphic textures of variable morphology have been produced experimentally in a wide range of mixed salt melts. Image analysis of 17 different textures described here using the ImageJ program (Rasband, 2015) gives 29 ± 4 mol% CaF_2 and 71 ± 4 mol% $CaCO_3$. Within the ternary system $CaCO_3$-CaF_2-$Ca(OH)_2$, the eutectic composition is 19 mol% CaF_2, 36 mol% $CaCO_3$, and 45 mol% $Ca(OH)_2$, yielding a dry mixture of 35 mol% CaF_2 + 65 mol% $CaCO_3$ (Gittins and Tuttle, 1964). Recent studies have shown cotectic crystallization of calcite and fluorite to occur between 620 and 553 °C, which corresponds to the ternary eutectic T with $Na_2Ca(CO_3)_2$ over the compositional range 58–72 mol% $CaCO_3$ (Tomkute et al., 2014). The composition of the intergrowths observed here is thus close to cotectic/eutectic compositions. Morphologically similar textures have been reported for eutectic melts in alkali earth-lanthanide-

Table 1B
Spreadsheet showing the model calculations for separation of fluoride melt from carbonate melt, followed by burbankite (Burb) and calcite crystallisation. All processes are assumed to follow Rayleigh fractionation behaviour. All compositional data are chondrite normalised (part B of Table 1).

	Fluorite separation					Burbankite crystalisation			Calcite crystallisation			
	Carbonate melt remaining					Carbonate melt remaining			Carbonate melt remaining			
	0.9	0.8	0.7	0.6	0.5	0.98	0.96	0.94	0.8	0.6	0.40	0.15
Carbonate melt composition												
La	11,441	12,862	14,689	17,123	20,527	4161	816	155	1002	1306	1897	4678
Ce	9449	10,624	12,134	14,146	16,961	3933	885	193	1085	1410	2042	4999
Pr	5028	5650	6448	7511	8996	2514	684	181	836	1084	1560	3771
Nd												
Sm	818	916	1041	1208	1439	606	251	102	304	390	552	1285
Eu												
Gd	302	337	381	439	520	360	247	169	296	373	516	1136
Tb												
Dy												
Y	101	85	69	55	42	41	40	39	48	60	83	181
Ho												
Er												
Tm												
Yb												
Lu	152	171	194	225	268	273	278	283	334	424	592	1328
Calcite melt composition												
La	910	1023	1169	1362	1633	331	65	12	80	104	151	372
Ce	824	926	1058	1233	1479	343	77	17	95	123	178	436
Pr	505	568	648	754	904	253	69	18	84	109	157	379
Nd												
Sm	114	127	145	168	200	84	35	14	42	54	77	179
Eu												
Gd	59	66	75	86	102	71	49	33	58	73	102	223
Tb												
Dy												
Y	21	17	14	11	9	8	8	8	10	12	17	37
Ho												
Er												
Tm												
Yb												
Lu	27	30	34	40	47	48	49	50	59	75	104	234

Please cite this article in press as: Kynicky, J., et al., The role of carbonate-fluoride melt immiscibility in shallow REE deposit evolution, Geoscience Frontiers (2018), https://doi.org/10.1016/j.gsf.2018.02.005

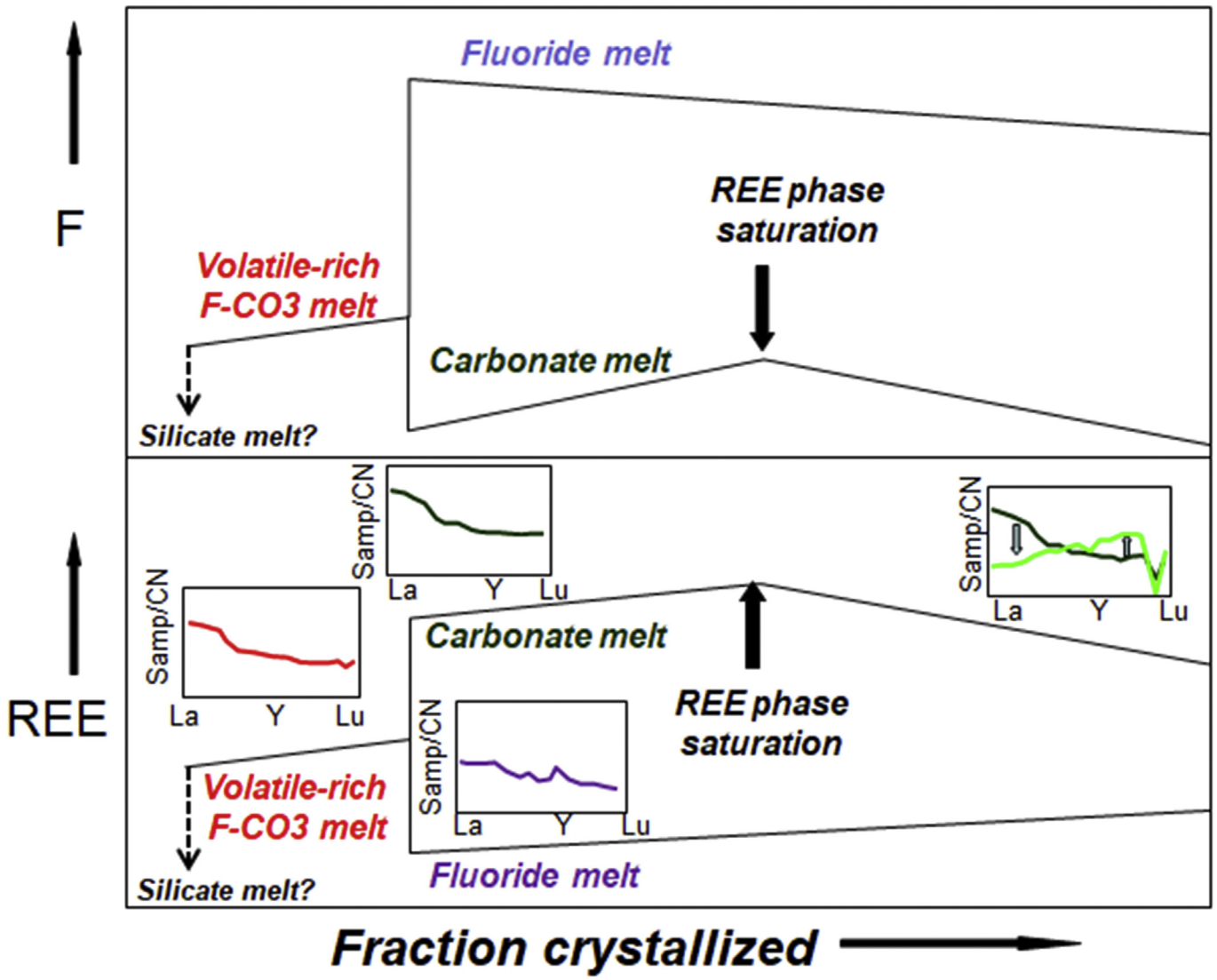

Figure 6. Conceptual model for melt evolution LuginGol, in terms of relative REE and F concentration in the melt. Chrondrite normalised REE pattern of crystallised mineral phases at various points in the system evolution are inset. We hypothesise a primary, volatile-rich alkali silicate magma, from which separated an F-rich, carbonate melt. This subsequently unmixed to produce a relatively REE-rich carbonate melt, and relatively REE-poor fluoride phase (fluorite or fluoride melt).

fluoride systems (Nafziger et al., 1976) and silicate-fluoride systems (Lin and Burley, 1969). Similar elongate structures have also been produced in NaCl-LiF eutectic melts by directional crystallization under carefully controlled temperature and stress gradients (e.g., Acosta et al., 2014). Crystallization of a fluoride-carbonate melt phase at cotectic or eutectic conditions is thus a possible mechanism for the formation of the textures observed in the present work. However, all the cited studies are experimental, with the textures produced by quenching of specifically eutectic compositions, and, in the case of the production of intergrowths for optical ceramics, obtained under very strongly controlled T and stress gradients. The Lugiin Gol textures occur in bands preceded and anteceded by pure calcite. Such a depositional sequence is difficult to reconcile with eutectic crystallisation and would require repeated inputs of carbonatitic magma. The surrounding textures are also not consistent with quenching. For the same reasons, cotectic crystallization cannot account for the localized occurrence of the Type 1 inclusions.

Thomas et al. (2012) have argued on the basis of melt inclusion studies that the conditions for the development of crystallization-controlled graphic intergrowths are unlikely to occur even in pegmatites, as they would require very low volatile activities, contrary to what is observed in natural systems. Consequently, these authors proposed a liquid immiscibility model, whereby the variable phase proportions and different surface tension and wettability of the two conjugate melts resulted in small droplets of the less abundant melt phase adhering to growth surfaces of crystals and thus becoming incorporated in the more voluminous fraction to form graphic intergrowths and microscale melt inclusions. The morphology of the spherical inclusions in this study closely resembles that of fluorite melt inclusions in quartz from Vasyukova and Williams-Jones (2014), albeit at larger scales. This, as well as the elongate amoeboid shape of the fluorite inclusions, suggests that the observed "graphic" textures could represent immiscibility between $CaCO_3$- and CaF_2-dominant melts. As noted above, carbonate-halide unmixing has previously been observed in melt inclusions (Panina, 2005) and natrocarbonatite lavas (Mitchell, 1997), although silicate-fluoride melt immiscibility has so far been reported only in alkali granite systems (Vasyukova and Williams-Jones, 2014). Analogous immiscibility between a hydrous, NaCl-

Please cite this article in press as: Kynicky, J., et al., The role of carbonate-fluoride melt immiscibility in shallow REE deposit evolution, Geoscience Frontiers (2018), https://doi.org/10.1016/j.gsf.2018.02.005

bearing carbonatite liquid and $CaCO_3$-rich hypersaline aqueous solution has been suggested on the basis of experimental data by Newton and Manning (2002). Such an origin is also supported by the compositional differences between fluorite from the calcite-fluorite intergrowths and coarse-grained fluorite elsewhere in the Lugiin Gol rocks (Fig. 5). However, it must be noted that the low REE content of the Type 2 fluorite inclusions is not consistent with its origin as an immiscible melt phase because fluoride melts would be expected to be REE-rich compared to virtually all other salt melts, and a melt phase formed by immiscibility would not be expected to be composed of pure CaF_2 (Veksler et al., 2012). In addition, it is not clear how such highly fluid ionic liquids as carbonate and fluoride melts would maintain their textural characteristics to and beyond the solidus. In experimental systems, low-viscosity liquids remain intermixed only in highly turbulent flows (Tadros, 2013), which may be applicable to the natrocarbonatitic lava of Mitchell (1997), but not to the Lugiin Gol dikes.

More or less similar calcite-fluorite intergrowth textures were discovered in other peralkaline complexes in Mongolia, especially in the case of Khalzan Buregte in Western Mongolia (Kempe et al., 2015), and Khan Bogd in South Mongolia (Kynicky et al., 2011). These intrusions of highly fractionated peralkaline syenitic or granitic systems lead to formation of REE, Nb and Zr deposits. The most mineralised parts of mentioned massifs are associated with the latest and the most evolved silicate rocks which contain up to 5 modal % of very similar intergrowth, involving pseudo-graphic intergrowths of fluorite and calcite in the small scale carbonatites and syenite-fluorite-calcite veinlets.

On the basis of current evidence, it is impossible to distinguish between the two potential models for the formation of the "graphic" calcite-fluorite textures. At the present time, we favour a model whereby a mixed carbonate-fluoride melt phase close to the cotectic/eutectic composition of Gittins and Tuttle (1964), separated immiscibly from a phonolitic melt, preferentially scavenging the REE and Zr. This melt subsequently crystallized a near-eutectic mixture of calcite and low-REE (but relatively HREE-enriched) fluorite, leading to passive enrichment of the residual carbonate melt in the REE, and particularly light lanthanides. This process provides a mechanism whereby REE-rich carbonatite could form by immiscibility, contrary to many current models (Le Bas, 1987; Harmer, 1999; Mitchell, 2005).

6.2. Preliminary model

If the calcite-fluorite intergrowth textures described above do represent the products of melt immiscibility, followed by cotectic to eutectic crystallization, then a simple model can be proposed to account for the evolution of calcite trace element composition. The calculations below are based on a conceptual model (Fig. 6), in which an F-rich carbonatitic melt separated from a volatile-rich silicate melt. Subsequent co-precipitation of calcite and fluorite produced a residual fraction saturated with respect to burbankite (at high Na and Sr activities in the parental melt) or REE ± Ca fluorcarbonates (predominantly synchysite), which lead to further fractionation and changes in the REE budget. The initial carbonate melt composition was calculated from calcite in the core of the intergrowths using a distribution coefficient ($K_d = C_{melt}/C_{solid}$) computed from the data of Dawson and Hinton (2003) and Klemme and Dalpé (2003). Because the reference data are only available for La, Ce, Pr, Sm, Gd and Lu, our model is limited to these elements. The same K_d's were also used to calculate the effects of calcite fractional crystallization. The fluorite-carbonate melt K_d was calculated from the mean fluorite composition and the least evolved carbonate melt composition. The carbonate melt-burbankite K_d was calculated from the mean burbankite composition and the initial carbonate melt composition. The overall model (Fig. 4) considers the composition of calcite precipitated following initial Rayleigh fractionation of fluorite from the parental carbonate melt, followed by burbankite, and then calcite crystallization in sequence. The calculations are based on the Rayleigh equation:

$$C_m = C_0(F^{(K_d-1)}) \quad (1)$$

where C_m is the concentration of an element in the residual melt at a specified melt fraction (F) separated by immiscibility, or removed by crystallization as calcite or burbankite, and C_0 is its concentration in the initial melt. The calculations simulated the change in the composition of calcite precipitated from magma undergoing fractionation of fluorite, followed by burbankite (used also as a proxy for fluorcarbonates), and then calcite. The REE patterns observed in the Lugiin Gol samples can be simulated by crystallization of up to 40 wt.% of fluorite (consistent with a calculated mole fraction of 23–27% fluorite), followed by precipitation of 6 wt.% of burbankite, and 85 wt.% crystallization of the remaining carbonate melt (Fig. 4).

The calculations imply that on separation of a carbonate-fluoride melt from its parental magma, the REE partitioned into the carbonate-fluoride melt phase and were subsequently concentrated in the carbonate melt. The experiments of Veksler et al. (2012) have demonstrated that the REE preferentially partition into a fluoride melt relative to its silicate conjugate, but not into a carbonate fraction separated from a silicate melt. However, their experimental results may not be applicable to more complex systems involving silicate-fluoride-carbonate mixtures. The presence of volatiles other than CO_2 has been shown to have a strong effect on REE partitioning in carbonate-silicate systems (Martin et al., 2013). The inferred composition of the carbonate-fluoride liquid in the present work (~14 wt.% F) would potentially provide a host into which the REE would partition preferentially to the conjugate silicate melt. Subsequent evolution of the derivative carbonatitic melt can only be speculated on because REE partitioning between fluorite and liquid in such igneous systems is not known. The low REE contents of the Lugiin Gol fluorite relative to the bulk carbonatite compositions appear to indicate partitioning of these elements in favour of the residual carbonatite magma. The few published studies of REE partitioning between fluorite and calcite in hydrothermal environments indicate one- to two-order-of-magnitude higher REE levels in the latter mineral (Schönenberger et al., 2008; Mondillo et al., 2016), but data on igneous fluorite in carbonatites are critically lacking.

The conditions of fluoride-carbonate melt separation from a volatile-rich silicate precursor have not been constrained. Panina (2005) determined that carbonate-chloride melt immiscibility takes place over a T range of 670–840 °C. Silicate-fluoride melt immiscibility occurs at T > 970 °C in dry systems (Dolejš and Baker, 2007), but at high H_2O activity may extend to 650 °C (Veksler et al., 2012). Vasyukova and Williams-Jones (2014) concluded that a fluoride melt separated from peralkaline granite and/or alkaline syenite at relatively high T, but the immiscibility persisted to as low as 650 °C. Silicate-carbonate melt separation may initiate at high temperature (>1200 °C; Panina, 2005), but is probably restricted to crustal depths (<10 kbar) and alkali-rich systems of phonolitic or nephelinitic composition (Brooker and Kjarsgaard, 2011). Field and petrographic evidence for Lugiin Gol, including the presence of explosive breccias with a fluorite matrix, and fluid inclusion microthermometry (Kynicky, 2006), suggests emplacement depths of 2 km or less, and thus is consistent with low-P (~0.5 kbar) conditions.

Please cite this article in press as: Kynicky, J., et al., The role of carbonate-fluoride melt immiscibility in shallow REE deposit evolution, Geoscience Frontiers (2018), https://doi.org/10.1016/j.gsf.2018.02.005

6.3. Implications

The observations, data and interpretations presented here extend the compositional range and nature of liquid-liquid immiscibility observed in nature at the meso- to macroscale, confirming previous interpretations based on microscopic observations of melt inclusions (Panina, 2005). The separation of a carbonate-fluoride melt from a volatile-rich syenitic precursor melt may play an important role in the evolution of alkali-silicate magmas, and, importantly, contribute to localized REE enrichment in these igneous systems. The subsequent formation of calcite-fluorite intergrowths suggests that the carbonate-fluoride melt was close to eutectic in composition. Further experimental work is required to determine if these textures were formed by co-precipitation of the two minerals, or by carbonate-fluoride liquid immiscibility. The mass-balance considerations require an initial carbonatite melt with ~14 wt.% F under either of the two alternative models. This level of F enrichment exceeds F concentrations documented in natural carbonatitic systems (e.g., ~8 wt.% F in natrocarbonatite from Oldoinyo Lengai, Tanzania: Gittins and McKie, 1980; Gittins et al., 1990). Experimental studies (Veksler et al., 2012), which show preferential REE partitioning into fluoride, but not carbonate, melts relative to their conjugate silicate fractions have been used to suggest that REE-rich carbonatites cannot be formed by immiscibility from silicate melts. The Lugiin Gol example indicates that separation of a mixed fluoride-carbonate melt phase may provide a mechanism for REE enrichment to occur via immiscibility at high F levels in the parental magma. The low REE partition coefficients for both igneous fluorite and calcite facilitate further REE enrichment of the carbonatitic magma through crystal fractionation.

7. Conclusions

Composite syenite-carbonatite dikes and veins at the Lugiin Gol complex host “graphic” intergrowths of calcite and fluorite. Mesoscale inclusions in calcite are either mixtures of fluorite, calcite and Na-Ca zirconosilicates, or pure fluorite. The intergrowths are composed of 29 ± 4 mol% CaF_2 and 71 ± 4 mol% $CaCO_3$, suggesting that their parental melt was close to the experimentally determined eutectic composition. This occurrence is the first reported macro-scale evidence for immiscibility between carbonate-fluoride and silicate melts. During the immiscible separation, the REE partitioned preferentially into the carbonate-fluoride fraction, whose subsequent evolution involved fractionation of relatively low-REE fluorite and produced calcite carbonatites hosting REE mineralization (fluorcarbonates + burbankite). The separation of an REE-enriched carbonate-fluoride melt from phonolitic magma is a hitherto unrecognized mechanism for REE-enrichment in carbonatites, and may play a role in the formation of shallow magmatic REE deposits. Further work is necessary to determine if the calcite-fluorite intergrowths observed in the present work represent products of eutectic crystallisation or were formed by another mechanism.

Acknowledgements

We thank editors and referees for their constructive reviews and editorial comments that led to improvements of manuscript. This work was supported by H2020 grant project (HiTech AlkCarb) and by project CEITEC 2020 (LQ1601).

References

Acosta, M.F., Ganschow, S., Klimm, D., Serrano-Zabaleta, S., Larrea, A., Merino, R.I., 2014. Directional solidification of the eutectic LiF-$LiYF_4$ using Bridgman and micro-pulling down techniques: microstructural study and some properties. Journal of the European Ceramic Society 34, 2051–2059. https://doi.org/10.1016/j.jeurceramsoc.2013.09.010.

Baatar, M., Ochir, G., Kynicky, J., Iizumi, S., Comin-Chiaramonti, P., 2013. Some notes on the Lugiin Gol, Mushgai Khudag and Bayan Khoshuu alkaline complexes, Southern Mongolia. International Journal of Geosciences 4 (8), 1200–1214. https://doi.org/10.4236/ijg.2013.48114.

Batbold, D., 1997. Mineralogy of the Carbonatite from the Lugiin Gol Alkaline Pluton. Unpubl. MSc thesis. Shimane University, Japan, 143 pp.

Bau, M., 1996. Controls on the fractionation of isovalent trace elements in magmatic and aqueous systems: evidence from Y/Ho, Zr/Hf, and lanthanide tetrad effect. Contributions to Mineralogy and Petrology 123, 323–333. https://doi.org/10.1007/s004100050159.

Bell, K., 1998. Radiogenic isotope constraints on relationships between carbonatites and associated silicate rocks – a brief review. Journal of Petrology 39, 1987–1996. https://doi.org/10.1093/petroj/39.11-12.1987.

Bell, K., Rukhlov, A.S., 2004. Carbonatites from the Kola Alkaline Province: origin, evolution and source characteristics. In: Wall, F., Zaitsev, A.N. (Eds.), Phoscorites and Carbonatites from Mantle to Mine: The Key Example of the Kola Alkaline Province, vol. 10. Mineralogical Society of Great Britain & Ireland, Mineralogical Society Series, pp. 433–468. https://doi.org/10.1180/MSS.10.

Best, M.G., 2003. Igneous and Metamorphic Petrology, second ed. Blackwell Publishing, Malden, USA. 729 pp.

Brooker, R.A., Kjarsgaard, B.A., 2011. Silicate-carbonate liquid immiscibility and phase relations in the system SiO_2–Na_2O–Al_2O_3–CaO–CO_2 at 0.1–2.5 GPa with applications to carbonatite genesis. Journal of Petrology 52, 1281–1305. https://doi.org/10.1093/petrology/egq081.

Castle, R.O., Lindsley, D.H., 1993. An exsolution silica-pump model for the origin of myrmekite. Contributions to Mineralogy and Petrology 115, 58–65. https://doi.org/10.1007/BF00712978.

Chakhmouradian, A.R., Smith, M.P., Kynicky, J., 2015. From “strategic” tungsten to “green” neodymium: a century of critical metals at a glance. Ore Geology Reviews 64, 455–458. https://doi.org/10.1016/j.oregeorev.2014.06.008.

Chakhmouradian, A.R., Wall, F., 2012. Rare earth elements: minerals, mines, magnets (and more). Elements 8, 333–340. https://doi.org/10.2113/gselements.8.5.333.

Cox, C., Kynicky, J., 2017. The rapid evolution of speculative investment in the 0REE market before, during, and after the rare earth crisis of 2010–2012. The Extractive Industries and Society. https://doi.org/10.1016/j.exis.2017.09.002.

Dawson, J.B., Hinton, R.W., 2003. Trace-element content and partitioning in calcite, dolomite and apatite in carbonatite, Phalaborwa, South Africa. Mineralogical Magazine 67, 921–930. https://doi.org/10.1180/0026461036750151.

Dingwell, D., Genova, D., Hess, K.U., Cimarelli, C., 2014. Viscosities of Highly Fluid Melts: Carbonatites and Analogues. AGU Fall meeting, V13C4807.

Dolejš, D., Baker, D.R., 2007. Liquidus equilibria in the system K_2O–Na_2O–Al_2O_3–SiO_2–F_2O_1–H_2O to 100 MPa: I. Silicate–fluoride liquid immiscibility in anhydrous systems. Journal of Petrology 48, 785–806. https://doi.org/10.1093/petrology/egm001.

Fenn, P.M., 1986. On the origin of graphic granite. American Mineralogist 71, 325–330.

Fulignati, P., Kamenetsky, V.S., Marianelli, P., Sbrana, A., Mernagh, T.P., 2001. Melt inclusion record of immiscibility between silicate, hydrosaline and carbonate melts: applications to skarn genesis at Mount Vesuvius. Geology 29, 1043–1046. https://doi.org/10.1130/0091-7613(2001)029<1043:MIROIB>2.0.CO;2.

Gittins, J., McKie, D., 1980. Alkalic carbonatite magmas: Oldoinyo Lengai and its wider applicability. Lithos 13, 213–215. https://doi.org/10.1016/0024-4937(80)90021-3.

Gittins, J., Beckett, M.F., Jago, B.C., 1990. Composition of the fluid phase accompanying carbonatite magma: a critical examination. American Mineralogist 75, 1106–1109.

Gittins, J., Tuttle, O.F., 1964. The system CaF_2-$Ca(OH)_2$-$CaCO_3$. American Journal of Science 262, 66–75. https://doi.org/10.2475/ajs.262.1.66.

Halama, R., Vennemann, T., Siebel, W., Markl, G., 2005. The Grønnedal-Ika carbonatite–syenite complex, South Greenland: carbonatite formation by liquid immiscibility. Journal of Petrology 46, 191–217. https://doi.org/10.1093/petrology/egh069.

Harmer, R.E., 1999. The petrogenetic association of carbonatite and alkaline magmatism: constraints from the Spitskop Complex, South Africa. Journal of Petrology 40, 525–548. https://doi.org/10.1093/petroj/40.4.525.

Kempe, U., Möckel, R., Graupner, T., Kynicky, J., Dombon, E., 2015. The genesis of Zr–Nb–REE mineralisation at Khalzan Buregte (Western Mongolia) reconsidered. Ore Geology Reviews 64, 602–625.

Klemme, S., Dalpé, C., 2003. Trace element partitioning between apatite and carbonatite melt. American Mineralogist 88, 639–646. https://doi.org/10.2138/am-2003-0417.

Kovalenko, V.I., Vladykin, N.V., Goreglyad, A.V., Smirnov, V.N., 1974. The Lugiingol massif of pseudoleucite syenite in the People's Republic of Mongolia (first find). Izvestia Akademie Nauk SSSR, Ser. Geol. 1974 (8), 38–49 (in Russian).

Kynicky, J., 2006. Carbonatites of South Mongolia. Unpublished PhD Thesis. Mendel University, Brno, p. 181.

Kynicky, J., Chakhmouradian, A.R., Xu, C., Krmicek, L., Galiova, M., 2011. Distribution and evolution of zirconium mineralization in perkalkaline granites and associated pegmatites of the Khan Bogd complex, southern Mongolia. Can. Mineral 49, 947–965.

Kynicky, J., Smith, M.P., Xu, C., 2012. Diversity of rare earth deposits: the key example of China. Elements 8, 361–367.

Le Bas, M.J., 1987. Nephelinites and carbonatites. In: Fitton, J.G., Upton, B.G. (Eds.), Proceedings of Rare Earths'04 MS. International Journal of Mass Spectrometry, vol. 253, pp. 87–97.

Lee, W.J., Wyllie, P.J., 1997. Liquid immiscibility between nephelinite and carbonatite from 1.0 to 2.5 Ga compared with mantle melt compositions. Contributions to Mineralogy and Petrology 127, 1–16. https://doi.org/10.1007/s004100050261.

Lee, W.J., Wyllie, P.J., 1998. Processes of crustal carbonatite formation by liquid immiscibility and differentiation, elucidated by model systems. Journal of Petrology 39, 2005–2013. https://doi.org/10.1093/petroj/39.11-12.2005.

Lin, S.B., Burley, B.J., 1969. The system CaF_2-$CaMgSi_2O_6$. Canadian Journal of Earth Sciences 6, 269–280. https://doi.org/10.1139/e69-024.

London, D., 2009. The origin of primary textures in granitic pegmatites. The Canadian Mineralogist 47, 697–724. https://doi.org/10.3749/canmin.47.4.697.

London, D., Morgan VI, G.B., 2012. The pegmatite puzzle. Elements 8, 263–268. https://doi.org/10.2113/gselements.8.4.263.

MacLellan, H.E., Trembath, L.T., 1991. The role of quartz crystallisation in the development and preservation of igneous texture in granitic rocks: experimental evidence at 1 kbar. American Mineralogist 76, 1291–1305.

Mariano, A.N., Mariano Jr., A., 2012. Rare earth mining and exploration in North America. Elements 8, 369–375.

Martin, L.H.J., Schmidt, M.W., Mattsson, H.B., Guenther, D., 2013. Element partitioning between immiscible carbonatite and silicate melts for dry and H_2O-bearing systems at 1-3 GPa. Journal of Petrology 54, 2301–2338.

Mitchell, R.H., 1997. Carbonate-carbonate immiscibility, neighborite and potassium iron sulphide in Oldoinyo Lengai natrocarbonatite. Mineralogical Magazine 61, 779–789. https://doi.org/10.1180/minmag.1997.061.409.03.

Mitchell, R.H., 2005. Carbonatites and carbonatites and carbonatites. The Canadian Mineralogist 43, 2049–2068..

Mitchell, R.H., Dawson, J.B., 2012. Carbonate–silicate immiscibility and extremely peralkaline silicate glasses from Nasira cone and recent eruptions at Oldoinyo Lengai Volcano, Tanzania. Lithos 152, 40–46. https://doi.org/10.1016/j.lithos.2012.01.006.

Mitchell, R.H., Kjarsgaard, B.A., 2008. Experimental studies of the system $Na_2Ca(CO_3)_2$ – NaCl – KCl at 0.1 GPa: implications for the differentiation and low-temperature crystallization of natrocarbonatite. The Canadian Mineralogist 46, 971–980. https://doi.org/10.3749/canmin.46.4.971.

Mondillo, N., Boni, M., Balassone, G., Spoleto, S., Stellato, F., Marino, A., Santoro, L., Spratt, J., 2016. Rare earth elements (REE) – minerals in the Silius fluorite vein system (Sardinia, Italy). Ore Geology Reviews 74, 211–224. https://doi.org/10.1016/j.oregeorev.2015.11.016.

Nafziger, R.H., Lincoln, R.L., Riazance, N., 1976. Fluoride flux systems for electroslag melting. In: Nafziger, R.H., et al. (Eds.), The Electroslag Melting Process: US Bureau of Mines, Bulletin, vol. 669, pp. 38–75.

Newton, R.C., Manning, C.E., 2002. Experimental determination of calcite solubility in H_2O-NaCl solutions at deep crust/upper mantle pressures and temperatures: implications for metasomatic processes in shear zones. American Mineralogist 87, 1401–1409. https://doi.org/10.2138/am-2002-1016.

Panina, L.I., 2005. Multiphase carbonate-salt immiscibility in carbonatite melts: data on melt inclusions from the Krestovskiy massif minerals (Polar Siberia). Contributions to Mineralogy and Petrology 150, 19–36. https://doi.org/10.1007/s00410-005-0001-3.

Pouchou, J.L., Pichoir, F., 1991. Quantitative-analysis of homogeneous or stratified microvolumes applying the model PAP. In: Heinrich, K.F.J., Newbury, D.E. (Eds.). Electron Probe Quantitation, Plenum Press, New York, pp. 31–75.

Rasband, W.S., 2015. ImageJ. U. S. National Institutes of Health, Bethesda, Maryland, USA, pp. 1997–2015. http://imagej.nih.gov/ij/.

Schairer, J.F., 1957. Melting relations of the common rock-forming oxides. Journal of the American Ceramic Society 40, 215–235. https://doi.org/10.1111/j.1151-2916.1957.tb12608.x.

Schönenberger, J., Köhler, J., Markl, G., 2008. REE systematics of fluorides, calcite and siderite in peralkaline plutonic rocks from the Gardar Province, South Greenland. Chemical Geology 247, 16–35.

Tadros, T.F., 2013. Emulsion formation, stability, and rheology. In: Tadros, T.F. (Ed.), Emulsion Formation and Stability. Wiley–VCH, Weinheim, Germany, pp. 1–75.

Thomas, R., Davidson, P., Beurlen, H., 2012. The competing models for the origin and internal evolution of granitic pegmatites in the light of melt and fluid inclusion research. Mineralogy and Petrology 106, 55–73. https://doi.org/10.1007/s00710-012-0212-z.

Tomkute, V., Solheim, A., Sakirzanovas, S., Øye, B., Olsen, E., 2014. Phase equilibria Evaluation for CO_2 Capture: CaO–CaF_2–NaF, $CaCO_3$–NaF–CaF_2, and Na_2CO_3–CaF_2–NaF. Journal of Chemical and Engineering Data 59, 1257–1263. https://doi.org/10.1021/je400999a.

Vasyukova, O., Williams-Jones, A.E., 2014. Fluoride–silicate melt immiscibility and its role in REE ore formation: evidence from the Strange Lake rare metal deposit, Que'bec-Labrador, Canada. Geochimica et Cosmochimica Acta 139, 110–130. https://doi.org/10.1016/j.gca.2014.04.031.

Veksler, I.V., 2004. Liquid immiscibility and its role at the magmatic–hydrothermal transition: a summary of experimental studies. Chemical Geology 210, 7–31. https://doi.org/10.1016/j.chemgeo.2004.06.002.

Veksler, I.V., Dorfman, A.M., Kamenetsky, M., Dulski, P., Dingwell, D.B., 2005. Partitioning of lanthanides and Y between immiscible silicate and fluoride melts, fluorite and cryolite and the origin of the lanthanide tetrad effect in igneous rocks. Geochimica et Cosmochimica Acta 69, 2847–2860. https://doi.org/10.1016/j.gca.2004.08.007.

Veksler, I.V., Dorfman, A.M., Dulski, P., Kamenetsky, V.S., Danyushevsky, L.V., Jeffries, T., Dingwell, D.B., 2012. Partitioning of elements between silicate melt and immiscible fluoride, chloride, carbonate, phosphate and sulfate melts, with implications to the origin of natrocarbonatite. Geochimica et Cosmochimica Acta 79, 20–40. https://doi.org/10.1016/j.gca.2011.11.035.

Wakita, H., Rey, P., Schmidt, R.A., 1971. Abundances of the 14 rare-earth elements and 12 other trace elements in Apollo 12 samples: five igneous and one breccia rocks and four soils. In: Proceedings of the Second Lunar Science Conference. Geochimica et Cosmochimica Acta Supplement, vol. 2, pp. 1319–1329.

Xu, C., Kynicky, J., Chakhmouradian, A.R., Li, X.H., Song, W.L., 2015. A case example of the importance of multi-analytical approach in deciphering carbonatite petrogenesis in South Qinling orogen: Miaoya rare-metal deposit, central China. Lithos 227, 107–121.

Please cite this article in press as: Kynicky, J., et al., The role of carbonate-fluoride melt immiscibility in shallow REE deposit evolution, Geoscience Frontiers (2018), https://doi.org/10.1016/j.gsf.2018.02.005